applied sciences

MDPI

Article

Design of a Novel RFID Reader for Oilwell Downhole Applications

Qixuan Hu, Yuesong Yang and Jixuan Zhu *

School of Automation, China University of Geosciences, Wuhan 430074, China; hqx031127@163.com (Q.H.); 14787783761@163.com (Y.Y.)
* Correspondence: zhujx@cug.edu.cn

Abstract: RFID (Radio Frequency Identification), which transmits control data through electronic tags in a non-contact manner, provides a new approach for efficient and low-cost remote control of oil downhole tools. However, the interference of harsh downhole environments and the high-speed movement of tags seriously affect the performance of the current downhole reader. To effectively address this issue, in this study, a novel downhole RFID reader is presented. By introducing the half-duplex communication protocol to replace the current full-duplex communication protocol in the hardware circuits of the reader, its tag recognition ability can be improved. Then, the corresponding hardware circuits and software programs are designed. Furthermore, a sparse solenoid antenna is adopted to replace the traditional tightly wound solenoid antenna, which can provide a longer reading area range to cope with the high-moving tag, and its total length and spacing parameters between adjacent coils are designed in detail. The test results show that the proposed RFID reader based on a half-duplex communication protocol can communicate with tags normally, and its sparse solenoid antenna provides significantly more tag reading times than traditional tightly wound solenoid antennas under the same antenna inductance.

Keywords: downhole oil well; RFID reader; half duplex; sparse solenoid antenna

Citation: Hu, Q.; Yang, Y.; Zhu, J. Design of a Novel RFID Reader for Oilwell Downhole Applications. *Appl. Sci.* **2024**, *14*, 7372. https://doi.org/10.3390/app14167372

Academic Editors: Paulo M. Mendes, Jose Cabral and Hugo Daniel da Costa Dinis

Received: 6 July 2024
Revised: 8 August 2024
Accepted: 9 August 2024
Published: 21 August 2024

1. Introduction

With the intensification of deep and ultra-deep efforts, conventional downhole tools and related technologies used in drilling and cementing operations are no longer fully meeting the needs of this field. As an emerging technology, radio frequency identification (RFID) is poised to offer a novel approach for efficient and cost-effective control of downhole tools through the contactless transmission of control data via electronic tags. Utilizing the principle of electromagnetic wave transmission, RFID offers operational simplicity, reliable data transfer, and ease of management and monitoring, enabling precise signal accuracy during downhole operations [1,2]. The RFID system typically comprises a downhole reader and an electronic tag. Notably, the reader's antenna is coaxially aligned with the metal drill pipe. When the electronic tag, carrying ground-based control instructions, moves into the antenna's vicinity with the borehole fluid, RFID communication captures the control instruction, thereby actuating the downhole tool [3], as shown in Figure 1. The application prospects for oil downhole RFID technology are exceptionally broad, promising substantial economic benefits.

The integration of RFID technology into oil well operations is a significant advancement in the petroleum industry, focusing on enhancing subsurface monitoring and data precision [4]. Sun et al. developed an RFID-based intelligent sub-control switch system for downhole valve operations [5]. Subedi et al. created a novel RFID reader localization method using signal strength from distributed passive tags [6]. Huang designed an RFID-driven downhole positioning device for accurate rescue positioning simulations [7]. Yu engineered an RFID-based downhole drilling tool monitoring system that tracks tool fatigue and collects asset information, improving condition monitoring and reducing downhole incidents [8]. Additionally, Mi developed an RFID-driven downhole traffic control system

that enhances operational efficiency and safety [9]. These studies leverage RFID technology to optimize production processes and real-time equipment monitoring, mitigating failure risks [10].

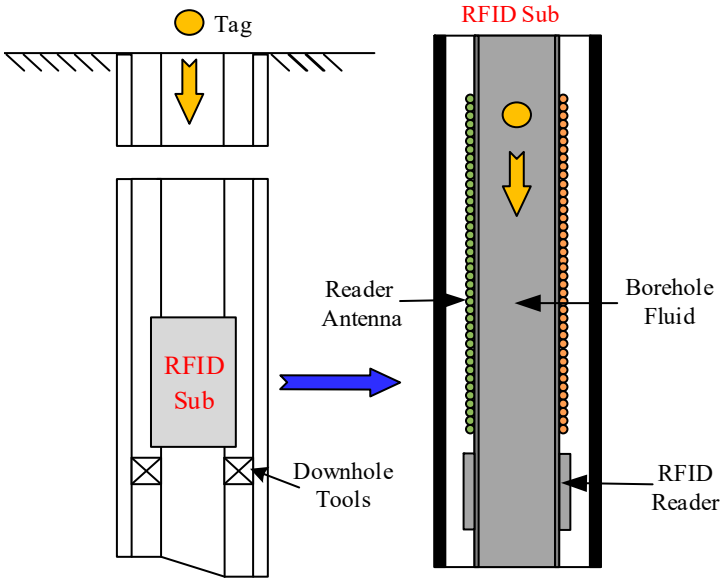

Figure 1. Downhole RFID system.

To further augment the wireless energy transmission capabilities of RFID technology, scholars have conducted an array of pertinent investigations. Geng et al. constructed a mathematical model elucidating the correlation between the various parameters of reader solenoid coils and executed computations to devise two types of reader coils capable of sustaining a continuous energy supply for electronic tags [11,12]. The empirical results revealed a 100% recognition rate for the reader with respect to dynamically moving electronic tags. Vyas et al. employed a passive RFID sensor platform to interrogate buried pipelines at depths up to 1.25 m within the low-frequency spectrum, facilitating health monitoring of magnetic carbon steel conduits [13]. Pérez-Nicoli et al. expanded the read range of near-field radio-frequency identification systems by introducing a resonating coil intermediate to the transmitter and receiver [14]. Zhu and colleagues presented an optimized design for RFID antennas and readers, ensuring dependable data acquisition and transmission under the harsh conditions of oil well production environments [15].

The predominant approach for most current downhole RFID readers adopts full-duplex (FDX) communication protocols. This necessitates that the RFID reader keep the antenna open continuously during data exchanges with electronic tags, which, however, leads to the tag return signal being easily mixed with downhole environmental interference. In addition, as the movement speed of the downhole tags is required to be faster, the current research on densely wound solenoid antennas requires a significant increase in antenna length, which increases the difficulty of impedance matching due to the large antenna inductance. Therefore, it is necessary to research and design a new downhole reader.

Different from the traditional downhole reader composed of an FDX reader circuit and a tightly wound solenoid antenna, this paper presents the design of a novel and new downhole reader. By introducing the HDX communication protocol in the hardware circuits of the reader, its tag recognition ability can be improved. In addition, by employing the sparse solenoid antenna, more tag reading times than traditional tightly wound solenoid antennas under the same antenna inductance can be provided. A comparison of the proposed reader with previous studies in the literature is shown in Table 1.

Table 1. Comparison of the Proposed Reader with Previous Studies.

Reference	[11,12]	[13]	[15]	This Work
Protocol	FDX	HDX	FDX	HDX
Frequency	125 kHz	134.2 kHz	125 kHz	134.2 kHz
Antenna	Tightly wound solenoid	Coil	Tightly wound solenoid	Sparse solenoid
Recognition Ability of Moving Tag	Low	Low	Low	High
Works in Downhole	Yes	No	Yes	Yes

2. Design of Downhole HDX Reader Hardware

2.1. Advantages of Half-Duplex Communication Protocols

The FDX communication protocol is a communication protocol that can send and receive data simultaneously, while the half-duplex (HDX) protocol is a distinctive communication protocol that allows data to be transmitted in both directions but only allows data to be transmitted in one direction at a time. HDX communication technology closes the reader's magnetic field during the return transmission of data. In contrast, FDX requires the reader's magnetic field to be kept open throughout the data transmission process. The HDX system, by closing its magnetic field upon data reception, allows readers to focus on tag signals more intensely, effectively eliminating the disruptive influence of the reader's RF field on these signals. This results in more accurate readings and a significantly reduced energy consumption when compared to FDX. Moreover, HDX adopts frequency-shift keying technology, which not only enhances the electromagnetic interference (EMI) robustness of HDX tags but also enables the reader the capability to accurately discern and differentiate between closely positioned tags.

In comparison to FDX, HDX streamlines the transmission process by trimming 3 bits from the data header and omitting control bits, thereby reducing the volume of transmitted data from 128 bits to a mere 112 bits. This compaction results in an enhancement of the transmission rate that approximates a doubling in efficiency. Therefore, adopting a HDX protocol instead of the current FDX protocol can help improve the tag recognition performance of the downhole RFID reader.

2.2. Hardware Design of HDX Reader

Considering the high temperature environment in the downhole, there is currently no corresponding temperature-resistant HDX integrated RF (Radio Frequency) chip available. Then, to implement the half-duplex communication protocol, it was decided in this RFID reader design to generate intermittent radio frequency signals by the microcontroller to simulate the half-duplex communication protocol. These signals are then power-amplified by a power amplifier and transmitted from both ends of the antenna. During the intervals when the radio frequency signals stop transmitting, signals from the electronic tags are received, demodulated using a demodulation circuit, and then sent to the microcontroller for processing. Based on the above discussion, the hardware block diagram of the RFID reader can be designed as shown in Figure 2.

In this design, Frequency Shift Keying (FSK) modulation is employed. FSK modulation refers to frequency modulation of the already modulated pulse waveform. FSK modulation is often used in cases where the frequency is below 135 kHz and exhibits strong anti-interference capabilities. Here, a modulation signal of 134.2 kHz is generated by the microprocessor and then amplified by the MIC4452 driver chip for power amplification before being transmitted to the antenna.

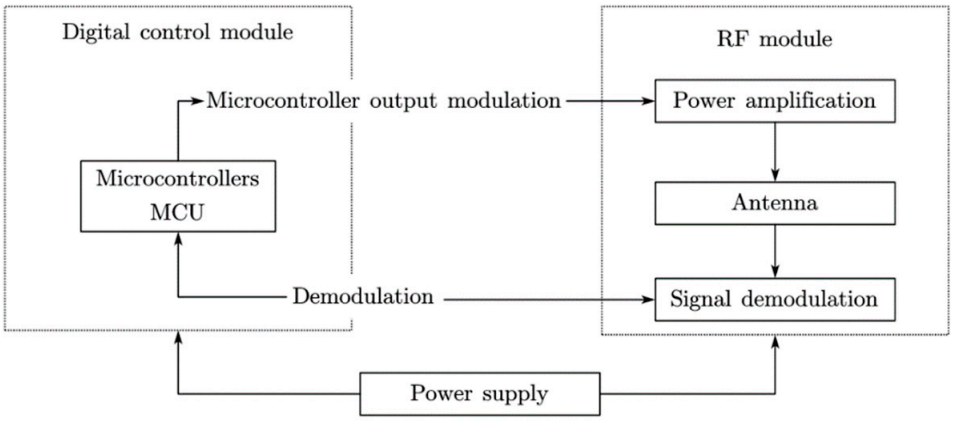

Figure 2. Hardware block diagram of RFID reader.

The MIC4452V is a high-performance, easy-to-use CMOS MOSFET driver known for its resistance to interference. Its features include a wide operating voltage range of 4.5 V to 18 V, a low delay time of 30 ns, and low output impedance. The operating temperature of the MIC4452VM ranges from −40 °C to +125 °C, with a power consumption of 1040 mW and a decay coefficient of 8.3 mW/°C. The circuit connection of the MIC4452 in the circuit is illustrated in Figure 3.

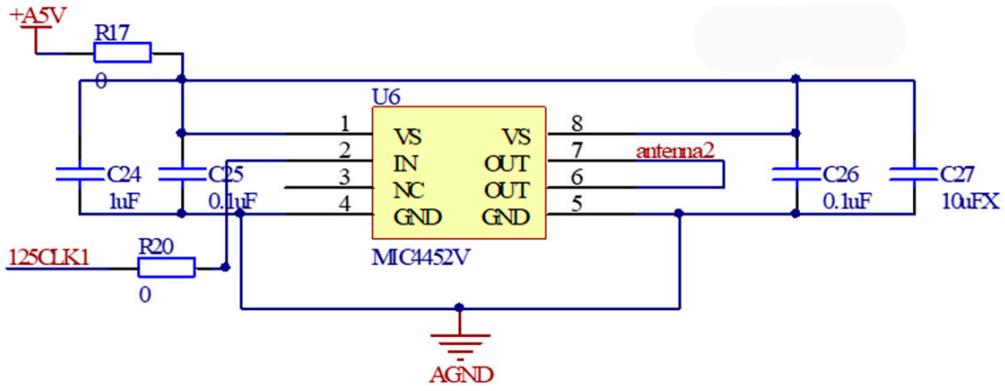

Figure 3. Circuit connection diagram of MIC4452.

After receiving data through the antenna, this design adopts the XR2211 chip for demodulation. The XR2211 is a FSK demodulator, utilizing a single-phase-locked loop system with a frequency range of 0.01 Hz to 300 kHz. The dynamic range of the input analog voltage ranges from 10 mV to 3 V. To enable the demodulation function of the XR2211, several resistors and capacitors in the peripheral circuit of the XR2211 need to be configured. Among the various models of XR2211, XR2211M operates within a temperature range of −55 °C to +125 °C, consumes 900 mW of power, and has a derating factor (Derate above 25 °C) of 5 mW/°C for Small Outline Integrated Circuit (SOIC) packaging.

According to the working principle of the XR2211, the demodulation circuit can be designed as shown in Figure 4. Based on the XR2211D chip manual and relevant information, the resistors and capacitors in the circuit can be calculated. Among them, the role of C15 and R9 is to set the PLL center frequency. Since the high level corresponds to a frequency of 124.2 kHz and the low level corresponds to a frequency of 134.2 kHz, the center frequency is 129.2 kHz. Therefore, R9 is set to 20 kΩ, and C1 is set to 360 pF. R13 is used to set the system bandwidth, set to 270 kΩ here, and C1 is used to set the time constant and damping factor of the loop filter, set to 91 pF here. C19 and R14 are used to filter the output data, with R14 set to 510 kΩ and C19 set to 310 pF. R10 acts as a pull-up resistor to raise the output voltage.

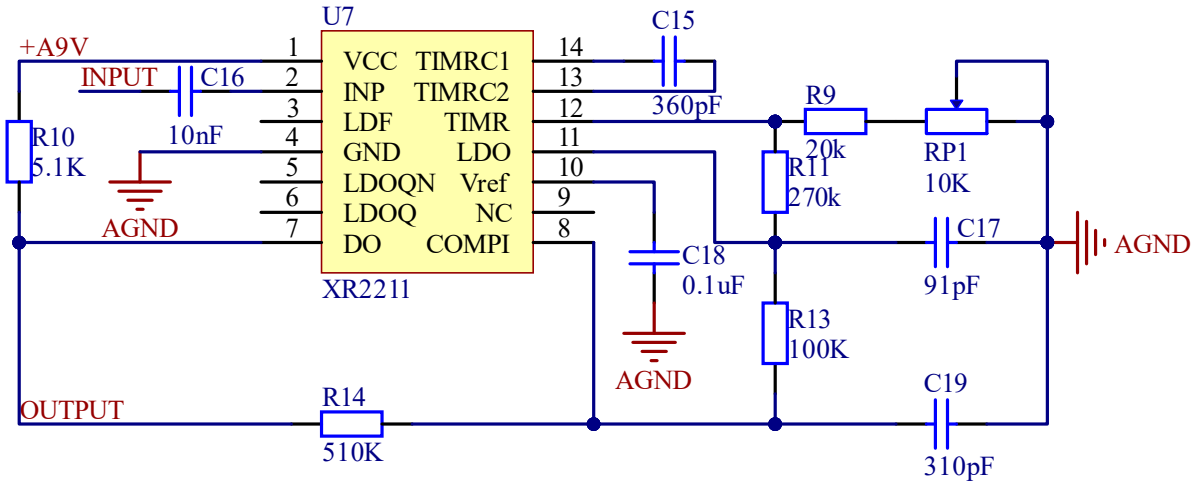

Figure 4. XR2211 demodulation circuit.

2.3. Software Design of HDX Reader

Considering that the electronic tags used for downhole communication have low requirements for storage space and control instructions, the electronic tag used in this design is RI-TRP-WR3P, produced by Texas Instruments Incorporated. RI-TRP-WR3P is a read-write electronic tag based on a semi-duplex communication protocol, with a length of approximately 23 mm and a weight of approximately 10 g. The operating temperature for read operations is −40 °C to 85 °C, and that for write operations is −40 °C to 70 °C. Charging for read-write operations requires a minimum of 15 ms, with a charging frequency of 134.2 kHz. During data read-write operations, RI-TRP-WR3P adopts FSK modulation to encode the signal, with a low-level frequency of 132.2 kHz to 136.2 kHz and a high-level frequency of 120.0 kHz to 128.0 kHz. Each level lasts for 16 radio frequency cycles, with a high-level time of approximately 120 us and a low-level time of approximately 128 us.

As the data encoding type returned by the RI-TRP-WR3P electronic tag is a non-return-to-zero code, a high level represents 1 and a low level represents 0, and a high level lasts for 120 us while a low level lasts for 128 us. The decoding flowchart is shown in Figure 5. In this decoding process, a variable-named temp is first set to store the time difference between two jumps, and then the temp is judged. When the data stored in the temp are approximately 8 consecutive high-level times at the beginning of the RI-TRP-WR3P electronic tag, the value of the startbit is set to 1 to start recording the data, and the first byte of the array is stored in 0xFF. Then, it is determined whether the time is triggered by the rising edge. If the rising edge is triggered, it represents the duration of the low-level data stored in the temp. Simply subtract one low-level time from the temp and move the data one bit to the left to save the data into the array. Then change the triggering method to ensure that the data in the next temp can be saved correctly. If the falling edge is triggered, it indicates that the data stored in the temp are of high-level duration. Simply subtract the high-level time from the temp and move the data one bit to the left and perform the OR operation with 0x01 to save the high level in the array. If the data stored in the array reach 112 bits, output the array and end the data collection, and then process the data.

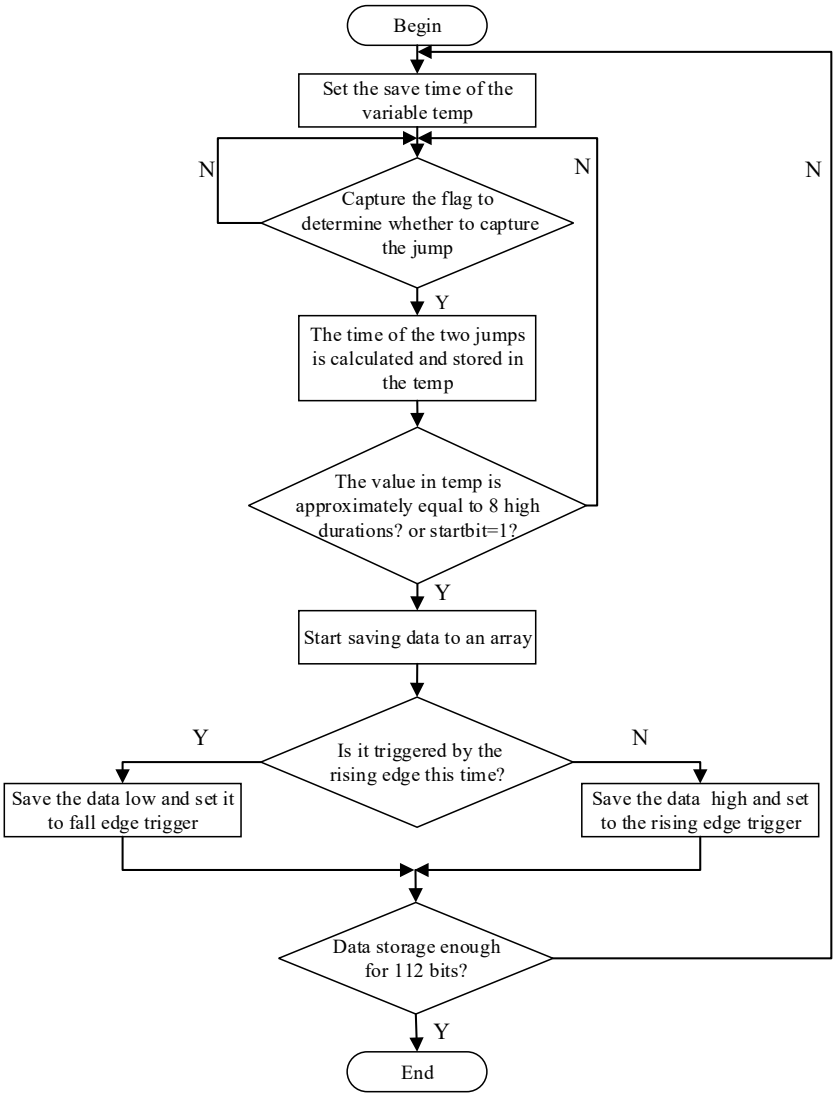

Figure 5. Decoding flowchart of tag data.

3. Design of Downhole RFID Sparse Solenoid Antenna

3.1. Magnetic Field Model of a Sparse Solenoid Antenna

Due to the rapid movement of electronic tags in underground oil pipelines, to capture complete data, it is necessary to extend the length of the solenoid antenna. However, a longer solenoid antenna will lead to an increase in its inductance value. Since the resonant matching capacitance cannot be made very small, it is necessary to reduce the antenna inductance by using a sparse solenoid antenna. The structure of the sparse solenoid antenna is shown in Figure 6, in which l represents the total length of the solenoid antenna, θ denotes the winding angle, a is the radial distance along the axis of the coil, and h is the spacing between adjacent windings.

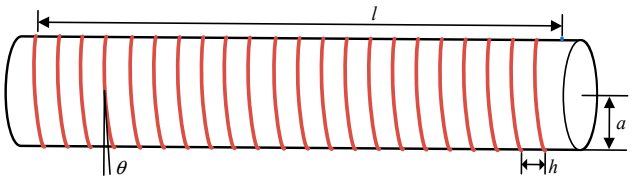

Figure 6. Sparse solenoid antenna structure.

According to Biot-Savart Law, the magnetic field distribution of a sparse solenoid coil antenna at any point in space can be derived as follows:

$$\begin{cases} H_x = \dfrac{I}{4\pi}\int_0^{2\pi z'/h} \dfrac{\left(az\cos\theta - a\dfrac{h}{2\pi}\theta\cos\theta - \dfrac{h}{2\pi}y + a\dfrac{h}{2\pi}\sin\theta\right)}{\left((x-a\cos\theta)^2 + (y-a\sin\theta)^2 + \left(z-\dfrac{h\theta}{2\pi}\right)^2\right)^{\frac{3}{2}}}d\theta \\ H_y = \dfrac{I}{4\pi}\int_0^{2\pi z'/h} \dfrac{\left(\dfrac{h}{2\pi}x - a\dfrac{h}{2\pi}\cos\theta + az\sin\theta - a\dfrac{h}{2\pi}\theta\sin\theta\right)}{\left((x-a\cos\theta)^2 + (y-a\sin\theta)^2 + \left(z-\dfrac{h\theta}{2\pi}\right)^2\right)^{\frac{3}{2}}}d\theta \\ H_z = \dfrac{I}{4\pi}\int_0^{2\pi z'/h} \dfrac{a(a - y\sin\theta - x\cos\theta)}{\left((x-a\cos\theta)^2 + (y-a\sin\theta)^2 + \left(z-\dfrac{h\theta}{2\pi}\right)^2\right)^{\frac{3}{2}}}d\theta \end{cases} \quad (1)$$

3.2. Parameter Impact Analysis of the Sparse Solenoid Antenna

According to (1), MATLAB can be used to analyze the effect of the magnetic field strength in various directions of the sparse solenoid, as well as the impact of the solenoid's total length and the spacing between adjacent windings on the magnetic field strength. It is assumed that the solenoid is in a vacuum medium, with a current of 30 mA flowing through the solenoid antenna, and the radius a of the solenoid antenna is 5 cm. When the spacing between adjacent windings is 0.5 cm and the total length of the solenoid antenna is 1 m, four points are taken within the solenoid for comparative analysis, and the calculated results are as shown in Figure 7.

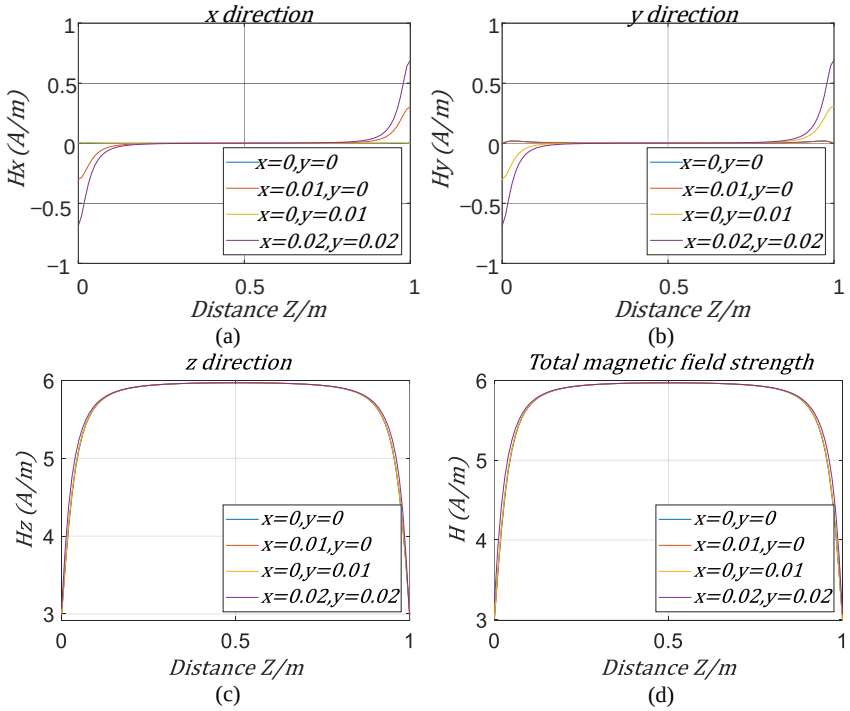

Figure 7. Magnetic field strength in various directions of the sparse solenoid antenna. (**a**) Hx, (**b**) Hy, (**c**) Hz, (**d**) Total magnetic field strength H.

It can be seen that the magnetic field strength in various directions of the solenoid antenna is different. The magnetic field strength in the x and y directions is close to 0, with only a slight increase at the ends of the solenoid, but this is also only at positions further away from the center of the xy plane of the solenoid. The magnetic field strength in the z direction is significant, especially in the middle part of the solenoid, where the z direction magnetic field reaches its maximum value. The total magnetic field strength curve and the magnetic field strength curve in the z direction basically coincide.

Based on the survey and analysis of electronic tags on the market, it can be found that the magnetic field strength of the currently available electronic tags on the market generally requires 5 A/m to fully return the data. Therefore, the analysis of the solenoid is conducted on the premise of setting the minimum magnetic field strength at 5 A/m. When analyzing the impact of the variation in the length of the solenoid on the magnetic field strength, the current flowing through the solenoid antenna is set to 30 mA, the radius a of the solenoid antenna is 5 cm, and the spacing between adjacent windings is 0.5 cm. Four points are taken in the solenoid for comparative analysis, and the calculation results are as shown in Figure 8. It can be observed that as the length of the solenoid increases, the total magnetic field strength of the solenoid also increases, but the change is relatively small. Considering various factors, this design adopts a sparse solenoid length of 0.8 m.

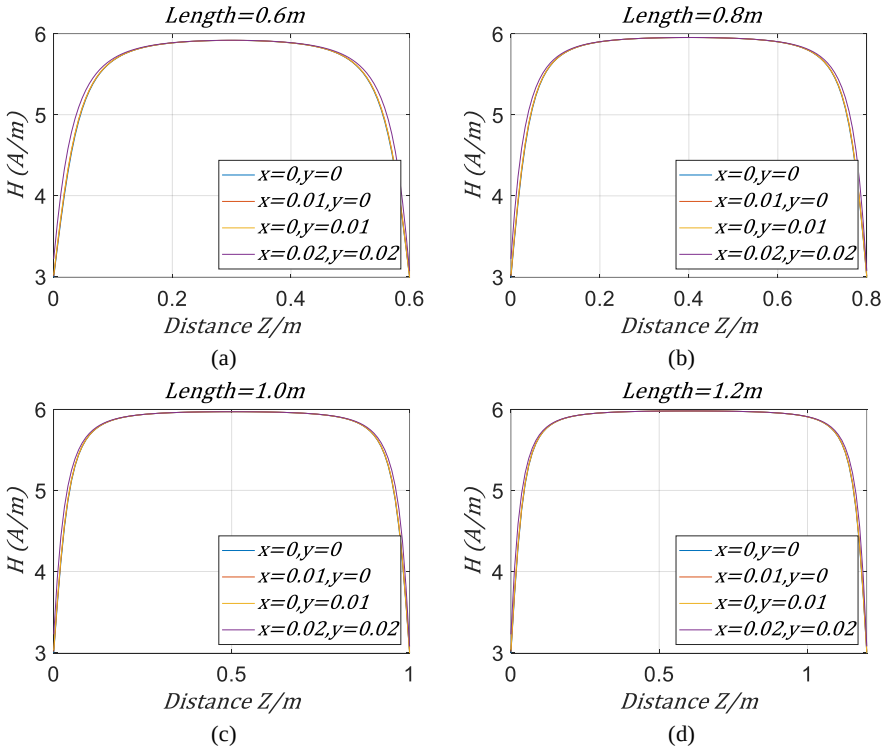

Figure 8. The effect of different antenna length on magnetic field strength. (**a**) l = 0.6 m, (**b**) l = 0.8 m, (**c**) l = 1.0 m, (**d**) h = 1.2 m.

When analyzing the impact of changes in the spacing between adjacent windings on the total magnetic field strength, the current flowing through the solenoid antenna is set to 30 mA, the radius a of the solenoid antenna is 5 cm, and the total length of the solenoid is fixed at 0.8 m. Four points are taken within the solenoid for comparative analysis, and the calculation results are as shown in Figure 9. The variation from 0.25 cm to 1 cm in the spacing between adjacent coils shows that the larger the spacing, the smaller the total magnetic field strength. Especially when the spacing increases from 0.25 cm to 0.5 cm, the magnetic field strength is halved. When the spacing between adjacent coils is greater than 0.75 cm, the total magnetic field strength will fall below 4 A/m. Therefore, in order to

activate the electronic tag by generating a total magnetic field intensity of more than 5 A/m in the solenoid antenna, the spacing between adjacent windings is selected as 0.5 cm.

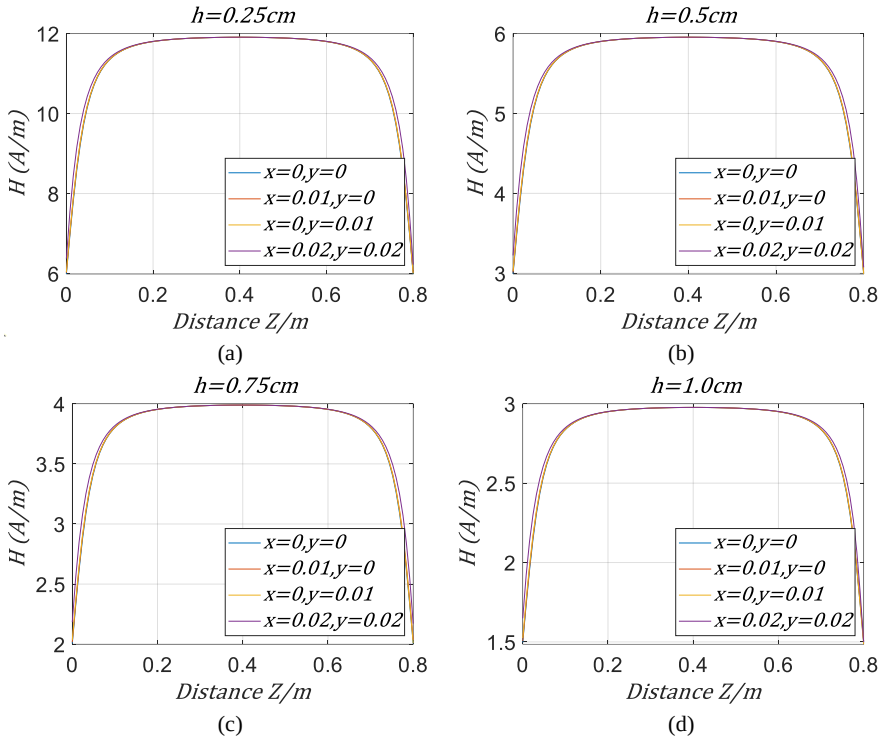

Figure 9. The effect of different adjacent winding spacing h on magnetic field strength. (**a**) h = 0.25 cm, (**b**) h = 0.5 cm, (**c**) h = 0.75 cm, (**d**) h = 1.0 cm.

4. Experimental Testing

To verify the proposed design, the experimental test system is implemented, as shown in Figure 10a, in which there is a simple downhole RFID system, including a designed HDX reader circuit, a sparse solenoid antenna, the commercial HDX microtags of RI-TRP-WR3P, and the battery. The length and the spacing between adjacent windings of the antenna is set to 0.8 m and 0.5 cm, respectively, based on the previous analysis. An oscilloscope of Tektronix DPO4104B is employed to measure the waveforms of the designed HDX reader circuit and the sparse solenoid antenna. As the signal modulation and demodulation module is a crucial part of the reader hardware circuit, the modulation signal generated by the microcontroller at 134.2 kHz is tested first. This signal, after being emitted from the microcontroller, is amplified by the MIC4452VM driver chip, and then applied to the reader antenna terminals. The waveform measured using an oscilloscope is shown in Figure 10b. It can be seen that one period is approximately 7.48 µs, with a frequency of 133.7 kHz and an error of less than 1%. Then, the signal demodulation testing is conducted. When the signal returned by the antenna enters the XR2211 demodulation chip, adjusting the center frequency of the XR2211 peripheral circuit allows for the output of a demodulated signal from Pin 7. This signal is in non-return-to-zero code. Measuring Pin 7 of the XR2211 with an oscilloscope yields the waveform depicted in Figure 10b. It can be observed that the data starts with a continuous high level of approximately 1000 µs, and there is also a continuous high level of approximately 1000 µs at the end, along with a consecutive 15-bit high-low level transition. According to the RI-TRP-WR3P electronic tag's chip manual, it can be inferred that the data are returned with full completeness and exhibit an accuracy rate of 100%. Therefore, the designed HDX RFID reader can communicate with tags normally.

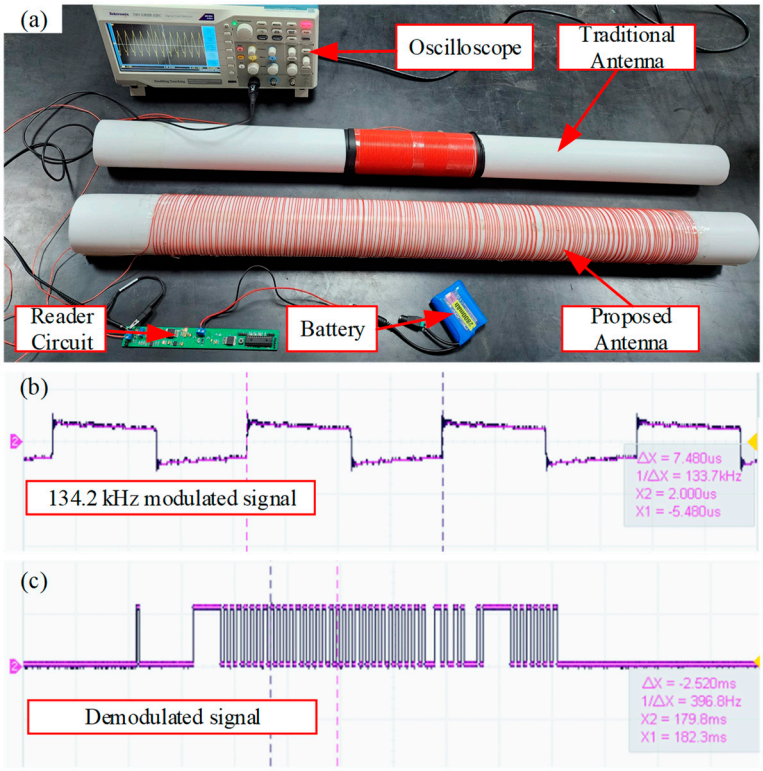

Figure 10. (**a**) Experimental test system. (**b**) 134.2 kHz modulated signal. (**c**) Demodulated signal.

Then, the performance tests of the sparse solenoid antenna are carried out; here, the traditional tightly wound solenoid antenna, which is often adopted as the reader antenna in the commercial downhole RFID system of Weatherford or the research of various downhole RFID systems, is employed for performance comparison. To avoid the influence of tag orientation on the reading times, the tag entered along the axial direction of the antenna. Considering the rapid movement of electronic tags with downhole fluids, it is evident that the longer the antenna length, the better in order to allow the electronic tag to stay in the reader antenna area for sufficient time to complete the data exchange. In other words, longer antennas can provide a greater number of tag reading times. The tag reading cycle is measured as 54 ms, as shown in Figure 11.

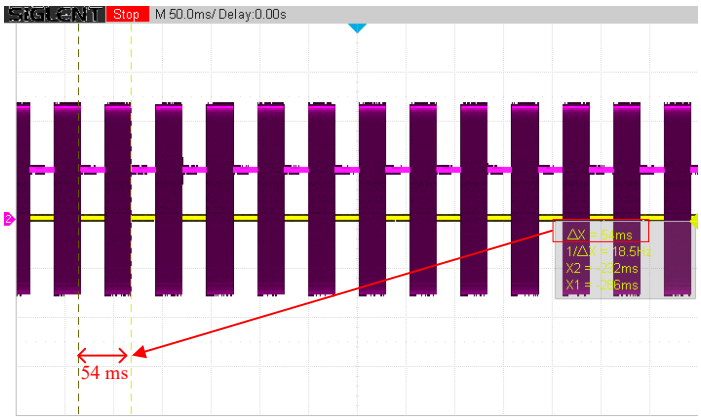

Figure 11. Measurement waveform of tag reading cycle.

For traditional tightly wound solenoid antennas, excessive antenna length will result in larger antenna inductance values and increase the difficulty of antenna impedance matching. Fortunately, the proposed sparse antenna with larger lengths do not have the

problem of large inductance. Using an impedance analyzer, the inductance of the designed sparse solenoid antenna with a length of 0.8 m was measured to be only 309 μH. The inductance value of a tightly wound antenna of the same length is 1.24 mH, which is nearly four times that of a sparse antenna. When the inductance value is the same, the length of the traditional tightly wound solenoid antenna is significantly reduced to 21 cm, which is much smaller than the length of a sparse solenoid antenna of 80 cm. A tag is put into the two vertically placed antennas in the form of a free fall, and the number of tag reading times can be measured with the oscilloscope, as shown in Table 2. It is obvious that the number of tag reading times of the proposed sparse solenoid antenna is much higher than that of traditional solenoid antennas, which is important for ensuring the reading reliability of high-speed moving tags in oil wells.

Table 2. Comparison of Number of Tag Reading Times for Two Antennas.

Antenna Type	Antenna Inductance	Antenna Length	Number of Tag Reading Times
Sparse solenoid antenna	309 μH	80 cm	13
Traditional solenoid antenna	313 μH	21 cm	4

5. Conclusions

In this study, a new HDX RFID reader with a sparse solenoid antenna for oil well applications is proposed to improve the reading reliability of high-speed moving RFID tags in complex downhole environments. Firstly, through hardware circuit design and software program design, a HDX RFID reader is implemented. Then, by analyzing the influence of antenna parameters on the magnetic field strength, the length and the spacing between adjacent windings of the sparse solenoid antenna are designed in detailed. The experimental results show that the designed HDX reader can achieve tag detection normally, and prove the usefulness of the proposed sparse solenoid antenna which can provide more reading times to detect rapidly moving RFID tags. In the future, we will optimize the parameters of the sparse solenoid antenna and compare the designed HDX reader with the traditional FDX reader to test their anti-interference performance.

Author Contributions: Conceptualization, Q.H. and J.Z.; methodology, Q.H. and J.Z.; software, Q.H.; validation, Q.H. and Y.Y.; formal analysis, Y.Y.; investigation, Q.H.; resources, J.Z.; data curation, Q.H. and Y.Y.; writing—original draft preparation, Q.H.; writing—review and editing, J.Z.; visualization, Q.H. and Y.Y.; supervision, J.Z.; project administration, Y.Y. and J.Z.; funding acquisition, Q.H. All authors have read and agreed to the published version of the manuscript.

Funding: This research received no external funding.

Institutional Review Board Statement: Not applicable.

Informed Consent Statement: Not applicable.

Data Availability Statement: The original contributions presented in the study are included in the article, further inquiries can be directed to the corresponding author.

Conflicts of Interest: The authors declare no conflict of interest.

References

1. Barandao, F.; Frreira, J.; Schwanke, D.; Breier, G.P.; Bove, C.N.; Bove, M.C.; Raposo, A.B. RFID technology as a life cycle management tool in the liquefied petroleum gas industry. *IEEE Lat. Am. Trans.* **2018**, *16*, 391–397. [CrossRef]
2. Liu, X.; Zhu, J. Oilwell downhole RFID reader based on discrete components. In Proceedings of the International Conference on Signal Processing and Communication Technology (SPCT), Harbin, China, 23–25 December 2022; Volume 12178, pp. 214–220.
3. Murdoch, E.; Valverde, E.; Sharma, R.; Wreden, C.; Goodwin, A.; Osei-Kuffour, J.; Kimmitt, K.; Loonstra, C.; Ghaempanah, B.; Reagins, D. Leveraging RFID Technology for Deepwater Drilling and Completions Challenges. In Proceedings of the SPE Intelligent Energy International Conference and Exhibition, Aberdeen, UK, 6–8 September 2016.

4. Mazeedi, M.; Hajri, A.; Amari, A. Design and implementation of an RFID system for downhole oil and gas applications. *J. Pet. Sci. Eng.* **2018**, *170*, 107–118.
5. Sun, H.; Bo, P.; Li, Z.; Hua, C.; Zhu, L.; MA, J. Development and Function Test of an Intelligent Split-Control Switch for Separate-Layer Oil Production. *Pet. Drill. Tech.* **2017**, *45*, 87–92.
6. Subedi, S.; Pauls, E.; Zhang, Y. Accurate Localization and Tracking of a Passive RFID Reader Based on RSSI Measurements. *IEEE J. Radio Freq. Identif.* **2017**, *1*, 144–154. [CrossRef]
7. Huang, S. Research on the application of RFID technology in downhole rescue positioning. *Coal Technol.* **2023**, *42*, 241–243.
8. Yu, Y. Research and application of RFID technology and automatic docking mechanism in key positions of air conditioning production. *Rrefrigeration* **2020**, *18*, 135–138.
9. Mi, Y. Application of precise positioning based downhole traffic light locking control. *Low Carbon World* **2024**, *14*, 73–75.
10. Cao, Y. Design and application of a coal mine downhole personnel positioning system based on radio frequency identification technology. *Mech. Res. Appl.* **2021**, *8*, 96–101.
11. Geng, S.; Gao, X.; Peng, X.; Bai, Y. Analysis and calculation of the effective length of a reader solenoid coil coupled to rapidly moving microtag. *IEEE Antennas Wirel. Propag. Lett.* **2018**, *17*, 894–897. [CrossRef]
12. Geng, S.; Hou, Y.; Chu, M.; Bai, Y.; Hou, L.; Wang, H. Analysis and computational methods for a reader solenoid coil used in industrial environments. *IEEE Trans. Ind. Electron.* **2019**, *67*, 3298–3306. [CrossRef]
13. Vyas, R.; Tye, B. A sequential RFID system for robust communication with downhole carbon steel pipes in oil and gas applications. *Electronics* **2019**, *8*, 1374. [CrossRef]
14. Pérez-Nicoli, P.; Rodriguez-Esteva, A.; Silveira, F. Bidirectional analysis and design of RFID using an additional resonant coil to enhance read range. *IEEE Trans. Microw. Theory Tech.* **2016**, *64*, 2357–2367. [CrossRef]
15. Zhu, J.; Tao, B.; Yin, Z. A customized RFID-based sensor system for intelligent oilwell. *IEEE Sens. J.* **2016**, *16*, 5426–5432. [CrossRef]